Title: Human interictal epileptiform discharges are bidirectional traveling waves echoing ictal discharges

Authors: Elliot H Smith[1,2*], Jyun-You Liou[3], Edward M Merricks[2], Tyler S Davis[1], Kyle Thomson[4], Bradley Greger[5], Paul A House[6], Ronald G Emerson[7], Robert R Goodman[8], Guy M McKhann II[9], Sameer A Sheth[10], Catherine A Schevon[2], John D Rolston[1]*

Affiliations:
[1]Departments of Neurosurgery and Biomedical Engineering, University of Utah, Salt Lake City, UT, USA; 84117.
[2]Department of Neurology, Columbia University, New York, NY, USA; 10032.
[3]Department of Anesthesiology, Weill Cornell Medicine, New York, NY, USA; 10065.
[4]Department of Pharmacology & Toxicology, University of Utah, Salt Lake City, UT, USA; 84117.
[5]Department of Bioengineering, Arizona State University, Tempe, AZ, USA; 85281.
[6]Neurosurgical Associates, LLC, Murray, UT, USA; 84107.
[7]Hospital for Special Surgery, New York, NY, USA; 10021.
[8]Lenox Hill Hospital, New York, NY, USA; 10075
[9]Department of Neurological Surgery, Columbia University, New York, USA; 10032
[10]Department of Neurosurgery, Baylor College of Medicine, Houston, TX, USA; 77030

*To whom correspondence should be addressed: John D Rolson (john.rolston@hsc.utah.edu), Elliot H Smith (e.h.smith@utah.edu), 175 N Medical Drive, Salt Lake City, UT, USA; 84117

Keywords: human, interictal, traveling wave, microelectrode array, epileptiform discharges, epilepsy, ictal, electrophysiology, ictal self-organization, neuroplasticity

Summary: Interictal epileptiform discharges (IEDs), also known as interictal spikes, are large intermittent electrophysiological events observed between seizures in patients with epilepsy. Though they occur far more often than seizures, IEDs are less studied, and their relationship to seizures remains unclear. To better understand this relationship, we examined multi-day recordings of microelectrode arrays implanted in human epilepsy patients, allowing us to precisely observe the spatiotemporal propagation of IEDs, spontaneous seizures, and how they relate. These recordings showed that the majority of IEDs are traveling waves, traversing the same path as ictal discharges during seizures, and with a fixed direction relative to seizure propagation. Moreover, the majority of IEDs, like ictal discharges, were bidirectional, with one predominant and a second, less frequent antipodal direction. These results reveal a fundamental spatiotemporal similarity between IEDs and ictal discharges. These results also imply that most IEDs arise in brain tissue outside the site of seizure onset and propagate toward it, indicating that the propagation of IEDs provides useful information for localizing the seizure focus.

Introduction

While seizures are mostly unpredictable and rare, electrical recordings from people with epilepsy often show isolated epileptiform discharges between seizures (Alarcon, 1997; de Curtis et al., 2012; Tatum et al., 2016). These IEDs are far more frequent, occurring up to several times per minute, and exhibit multidien variation in their frequency that correlates with seizure likelihood, making IEDs an attractive personalized biomarker for seizure risk *(Baud et al., 2018)*. Beyond such temporal information about seizure occurrence, there is some evidence for overlap between cortical areas where seizures originate and those with more IEDs *(Alarcon, 1997; Conrad et al., 2020; Marsh et al., 2010)*. Furthermore, some retrospective studies showed that removing brain areas with more IEDs improved surgical outcomes in patients with medically refractory epilepsy *(Kim et al., 2010; Smart et al., 2012)*. Despite these findings, the long-debated relationship between IEDs and seizure generating tissue remains unresolved (de Curtis et al., 2012; Paolicchi et al., 2000; Tonini et al., 2004; Vakharia et al., 2018).

Microelectrode array recordings in epilepsy patients have revealed the spatiotemporal features of ictal self-organization (Eissa et al., 2017; Martinet et al., 2017; Merricks et al., 2020; Schevon et al., 2012a; Smith et al., 2016). These studies reported two classes of recordings, one in which neuronal firing is recruited into the ongoing seizure, and another in which neuronal firing is relatively unaffected, despite seizure-like field potentials appearing on the same microelectrodes. These classes correspond to two dynamically evolving regions known as the ictal *core* and *penumbra*, respectively *(Schevon et al., 2012a)*. A slowly-propagating, narrow band of tonic action potential firing, the ictal wavefront (IW), delineates the transition between the core and penumbra *(Martinet et al., 2015; Schevon et al., 2012a; Trevelyan et al., 2007, 2006)*. These dynamic seizure regions exhibit distinct spatial features. The slowly traveling IW repetitively emits rapidly traveling ictal discharges backwards, toward the seizure core. These discharges occur following the passage of the ictal wavefront and have thus been termed post-recruitment discharges (Smith et al., 2016). In some patients, earlier ictal discharges, termed pre-recruitment, are also emitted outward, toward the penumbra *(Martinet et al., 2017; Smith et al., 2020, 2016)*. To avoid confusion between ictal discharges and interictal discharges, we will from here on refer to ictal discharges as seizure discharges (SDs).

The discovery of these spatiotemporal features of human seizure activity inspired a computational model designed to explain the neuronal underpinnings of seizure dynamics from biophysical principles *(Liou et al., 2020)*. After several induced seizures in this model, the network produces spontaneous seizures and IEDs with spatiotemporal dynamics. One prediction of the model is that the repeated barrages of traveling synaptic activity during SDs eventually coopt mechanisms of synaptic plasticity, biasing local tissue to propagate IEDs in similar directions as SDs, that is in the opposite direction of the slow propagation of seizure expansion. In this study we test the resultant hypothesis that IEDs have a predominant direction of propagation, towards the site of seizure onset; opposite the direction of seizure expansion. We found that the data supported this hypothesis, and further, that in the majority of participants, IEDs traveled bimodally on a linear axis with predominant and auxiliary sub-distributions whose directions, speeds, and proportions echoing those of SDs. Finally, we directly quantified the extent to which IED directions could be used to predict SD directions.

Results

IED detection in human microelectrode array recordings

To examine the spatiotemporal propagation of IEDs, we used a multi-institutional dataset of Utah-style microelectrode array (UEA; 10 X 10 microelectrodes in 4 X 4 mm grid, penetrating 1 mm) recordings from 10 epilepsy patients (2 female, $\mu \pm \sigma$ age: 29 ± 5.24 years) undergoing monitoring for neurosurgical treatment of medically refractory epilepsy (clinical details in Extended Table 1). In order to capture seizures (2.2 ± 1.6 seizures recorded per participant; 22 total), we recorded data continuously throughout the patients' monitoring periods (Figure 1A; 4.3 ± 2.4 days per participant; 43 total). Searching through weeks' worth of microelectrode data, we detected 45,623 candidate IEDs across the 10 participants (4,562.3 ± 5,171.7 per participant) using an IED detection algorithm designed for microelectrode recordings, that operated on features of IEDs based on the American Clinical Neurophysiological Society's definition, namely high-amplitude bursts of beta-range (20-40 Hz) local field potential (LFP) power occurring across multiple microelectrodes (Fig. S1; Algorithm S1) *(Tatum et al., 2016)*. Using this algorithm, we detected an average of 0.43 ± 0.51 IEDs per minute. The UEA enabled us to record both LFP data and multiunit action potential firing (MUA) across high-density spatial grid during each IED. These features of an example IED are shown in Figure 1C-G.

IEDs propagate in predominant and auxiliary directions

In order to determine whether the detected IEDs were traveling waves, and to measure wave speeds and directions, we fit a plane to the timings of both IED voltage extrema and MUA event times measured on each microelectrode using multi-linear regression *(Liou et al., 2017)*. IEDs with regression slopes that were significantly different from zero were classified as traveling waves (permutation test against a distribution of 1000 spatially permuted timings; Fig. 1H, Fig. S2). Traveling wave speeds and directions were then derived from each significant model's slope. Based on this operational definition, 30,278 IEDs (3,027.8 ± 3,190.0 per participant) were classified as traveling waves (66.4%).

Summary statistics for the spatiotemporal features of IEDs are shown in Table 1. IED speeds were on the same order as SDs before the passage of the ictal wavefront *(Liou et al., 2017; Smith et al., 2016)*. Traveling waves were also detected from MUA, independent of LFP recordings, though at a slightly reduced rate (2,215.7 ± 3,237.6 per participant; 22,157 total; 48.6%; χ^2 = 2957, $p < 0.05$). This result was expected, as LFP is a more reliable signal to record, and action potential firing during IEDs has previously been shown to be remarkably heterogeneous, particularly in areas further from the seizure onset zone *(Keller et al., 2010)*. That there were significantly more IED traveling waves in UEA recordings that were eventually recruited into the seizure core, further supports the idea that more firing, closer to the seizure onset zone improves reliability of traveling wave detection with MUA (McNemar Test, $\chi^2(1) = 2957,\ p < 10^{-6}$). We therefore focus our analysis on IED traveling waves measured from LFP minima in order to understand IED propagation across participants.

Having determined the majority of IEDs met the criteria to be classified as traveling waves, we next sought to understand whether IEDs from each participant exhibited a predominant propagation direction. We therefore tested whether distributions of IED traveling wave directions deviated from a uniform circular distribution *(Fisher, 1953)*, we found that each participant's IED traveling wave distribution exhibited a dominant direction (Fig. 2A; Hermans-

Rasson Tests, 1000 permutations, all $p < 10^{-3}$). These results show that many IEDs are traveling waves with predominant, consistent directions of travel in each participant.

In addition to a predominant direction common to all participants, many participants appeared to have a second, auxiliary, distribution of IED directions. We therefore fit each participant's IED distribution into a mixture of two circular normal sub-distributions (von Mises distribution). The mixture model was compared to a single von Mises distribution model by using permutation-based Kuiper tests (see **Materials and Methods**). IED traveling wave distributions were thus classified as bimodal in 8 of the 10 participants (Figure 2B). The mean and s.d. angles between the two IED sub-distributions was 177.9 and 10.7 degrees, respectively (Figure 2C). These results show that IEDs also frequently propagate antipodally to their predominant direction, suggesting that IEDs may travel both directions on a linear track through a fixed recording site.

Spatial features of IED distributions echo ictal self-organization

We next sought to understand whether IED speed and direction related to the spatial self-organization of seizures. We hypothesize that spatial features of IED traveling waves would correlate with seizure propagation direction and those of seizure discharges. We therefore measured the spatial features of seizures first. Fast and slow spatial features of focal seizures were measured in both ictal LFP and MUA bands as in previous reports *(Liou et al., 2017; Schevon et al., 2012a; Smith et al., 2016)*. Both of these features were measured using the same multilinear regression framework used to measure IED speed and direction.

Following previous reports with microelectrode arrays, we confirmed that seizures could be divided into two classes based on ictal recruitment: "recruited" and "penumbral" (see **Materials and Methods**; *14, 24, 25)*. Recruited tissue exhibited a slow expansion of tonic neuronal firing, the ictal wavefront (Fig. 3D-E; Fig. S4A-D), followed by rapidly traveling SDs (Movie S1). Penumbral tissue showed neither an IW nor repetitive SDs associated with phase-locked firing (Fig. S4E-H). Six participants' microelectrode arrays were recruited into the ictal core (10 seizures; Fig. 3A-C), while the four remaining participants were penumbral (12 seizures, Fig. S4E-H).

As predicted by our theoretical work *(Liou et al., 2020)*, similar patterns of IED and SD propagation were apparent in the majority of seizures in participants with "recruited" seizures. The majority of IEDs travelled opposite the direction of seizure expansion (i.e., the IW; direction difference from IEDs = 148.9 ± 17.2 degrees; median tests between IW and IED distributions, all $p < 0.05$; Fig. 3F). Moreover, IEDs traveled in similar directions as SDs in these participants (example in Fig. 3G; mean ± s.d. angle difference across participants = 23.7 ± 33.7 degrees). Direction distributions for IEDs, SDs, relative to the direction of the ictal wavefront are shown for all "recruited" participants in Figures 4A-F, and direction summaries for these participants are shown in Figures 4G-H (raw directions shown in Fig. S5). In the "penumbral" category, where the tissue under the UEAs were not obviously recruited from adjacent cortex as in the "recruited" category, we could not reliably detect or measure the direction of seizure expansion.

In order to directly quantify information about the full distribution of SDs that is gained from observing IEDs, we measured the Kullback-Leibler Divergence (KLD) between IED and SD distributions for each participant. The $\mu \pm \sigma$ KLD across these 10 seizures was 0.66 ± 0.56, and are shown next to each pair of distributions in orange in Figure 4. These results indicate that less than one extra bit of information is needed to encode the direction of SDs with IEDs on average, suggesting that IED directions could be used to accurately predict SDs.

Spatial features of IED sub-distributions predict those of SD sub-distributions

Finally, we sought to further understand geometric features of bimodal IED distributions and how they related to patterns of SD propagation. Such an understanding was only relevant for the "recruited" participants with bimodal IED distributions (5 participants, 7 seizures). Using the same bimodality classification strategy as for IEDs, we found that 5 of the 7 these seizures in these participants exhibited bimodal SD distributions, with similarly antipodal sub-distribution directions (Fig. 5A-B; $\mu \pm \sigma$ angle difference = 135.2 ± 24.6). Only participants with bimodal IED distributions had bimodal SD distributions, and only one participant, who had the least bimodal IED distribution, did not have clearly bimodal SDs.

In order to determine whether IEDs in each sub-distribution came from neurophysiologically distinct IED populations, we tested for differences between IED waveforms and firing rates between IED sub-distributions. Such differences might indicate that each IED sub-distribution reflected a separate population of IEDs propagating across the footprint of the UEA. However, neither firing rates nor IED waveforms differed between IED sub-distributions (Fig. 5C-D; cluster-based permutation tests, all $p > 0.05$), indicating that neither IED waveforms nor firing rates between the two sub-distributions could be statistically distinguished.

The aforementioned results indicate that both SDs and IEDs propagate antipodally through the same tissue. Differences between speeds and proportions of IED sub-distributions, corresponding to those we previously showed in SD sub-distributions *(Smith et al., 2016)*, would support a learned relationship between IEDs and SDs, as predicted by the centripetal pattern of learning in the theoretical model *(Liou et al., 2020)*. To address this question, we tested for differences in speed and relative size of SD and IED sub-distributions. Speeds were significantly different between IED sub-distributions within each participant (Fig. 5E; Mann-Whitney U, all $p < 10^{-4}$). Speeds were also significant between SD sub-distributions in five of the seven seizures (Fig. 5E; Mann-Whitney U, $p < 0.04$ in 5 seizures; $p > 0.62$ in two seizures). Finally, the proportion of IED directions in each sub-distribution predicted the direction of each SD sub-distribution in four of the five participants (two sample proportion tests, $\chi^2 > 347.6$, $p < 10^{-6}$). More pre-recruitment discharges occurred in a fifth patient with nearly equivalent proportions of IEDs across sub-distributions. Importantly the directions of significant differences in these spatial features corresponded across IED and SD sub-distributions. These results show that when IED and SD distributions were bimodal, their spatial features were similar, underscoring the extent to which IEDs mimic spatiotemporal features of ictal self-organization.

Discussion

Our results, using microelectrode array recordings in patients with epilepsy, show that IEDs are traveling waves that echo – and are predictive of – the propagation patterns of SDs, along an axis intersecting the seizure core. It is likely that the frequent barrages of coordinated activity seen during seizures—SDs—potentiate propagation pathways through neocortex that are revisited during IEDs. This hypothesis is corroborated by the predictions of our theoretical work, where a computational model incorporating spike-timing dependent plasticity and realistic connectivity between inhibitory and excitatory cells self-organized to produce IWs, SDs, and IEDs that echo through the pathways potentiated by the strong, repeated barrages of SD activity, antipodal to the IW *(Liou et al., 2020; Nguyen et al., 2020)*. Therefore, these results suggest that the predominant IED direction could be used to localize the seizure source. Moreover, the empirical results reported here extend our understanding of the geometric properties of epileptic tissue, beyond the model predictions, in showing that IEDs travel largely bidirectionally on a linear axis. The bidirectional propagation of IEDs is similar to the bidirectional traveling waves we have previously observed during seizures *(Liou et al., 2017; Smith et al., 2016)*. The bidirectional pattern of traveling waves during seizures emanated from a slowly expanding, motile source of ictal activity—the IW—passing through a fixed recording site *(Smith et al., 2016)*. The data presented here show that IEDs travel in similarly oriented, bimodal distributions, even in the absence of an IW or ictal self-organization.

The theoretical model predicted that the directional preferences of IEDs were learned from SDs via spike-timing dependent plasticity *(Bi and Poo, 1998)*. While we cannot address the specific learning mechanism with this dataset, in participants whose UEAs were recruited into the seizure core from adjacent cortical tissue, we showed correspondences between several spatial properties of IEDs and SDs. The speeds, directions, and relative sizes of IED sub-distributions echoed those of SDs. Moreover, predominant IED and SD directions opposed the directions of the ictal wavefronts in "recruited" UEAs. These relationships were unable to be determined from UEAs that were not recruited into the seizure core ("penumbral" recordings). Together, these results suggest that spatiotemporal biases exist in epileptic tissue. Whether spatiotemporal biases in IEDs arise from learning during SDs or vice versa remains to be determined. While the theoretical model indicates that several seizures must occur before IEDs begin to form, electrographic discharges, similar to IEDs, often appear before seizures in animal models of epilepsy *(Staley et al., 2011)*.

While we show that the majority of IEDs are traveling waves whose directions overlap with those of SDs, it is important to recognize the small spatial scale of the recordings analyzed here. Additional, more eccentric populations of IEDs could be propagating from distant areas that are connected to the seizure onset zone, though not necessarily from adjacent tissue on the cortical surface *(Gelinas et al., 2016)*. Higher density ECoG that spans a larger cortical territory than the UEA would be useful in gaining more context on where IEDs arise, and how IEDs propagate across the cortical surface. On the other hand, there is currently no evidence that the ictal wavefront can be detected without action potential recordings, though the time of seizure recruitment can be roughly estimated on each ECoG electrode from high-frequency LFP *(Smith et al., 2020; Weiss et al., 2013)*. Precise IED propagation patterns are also difficult to measure with the relatively low sampling density of ECoG. Animal studies using calcium indicators capable of imaging neuronal activity across large cortical territories may overcome these limitations *(Liou et al., 2019; Wenzel et al., 2017)*. Such animal studies are also poised to understand how learning and plasticity contributes to the geometric relationships reported here.

While these microelectrode array recordings inform fundamental geometric relationships between IED propagation and ictal self-organization, additional spatial context may inform our understanding of "penumbral" tissue *(Smith et al., 2020)*. Future work will therefore focus on translating these microelectrode array results to a more clinically relevant spatial scale. For example, using ECoG *(Khodagholy et al., 2014; Viventi et al., 2011)* with vector field or convolutional methods *(Muller et al., 2016)*, or examining propagation of source-localized IEDs in stereo-EEG. Such approaches will be useful for linking the micro results reported in this paper to the coarser spatial resolutions and broader coverages encountered with typical intracranial recordings. Integrating these multi-scale geometrical understandings of how IEDs relate to the seizure onset zone could then provide an additional piece of information to inform diagnosis and treatment of medically refractory epilepsy, and potentially enable localizing the seizure source without having to directly observe seizures.

Acknowledgments: Thanks to the Schevon and Rolston labs. This work was supported by NIH NINDS R21 NS113031 (J.D.R.), NIH NINDS K23 NS114178 (J.D.R.), NIH S10 OD018211 (C.A.S.), NIH R01 NS084142 (C.A.S.), and a Junior Investigator Award from the American Epilepsy Society (E.H.S.).

Author contributions: EHS, JYL, CAS, and JDR conceived of the experiments. EHS, EMM, TSD, KT, BG, PH, RGE, RRG, GMM, SAS, and CAS were involved with data collection. EHS, JYL, and EMM analyzed the data. EHS, JYL, and JDR wrote the manuscript. All authors provided edits to the manuscript.

Declaration of interests: The University of Utah has a financial interest in the company that makes the Utah microelectrode array. Dr. Rolston reports personal fees from Medtronic. Dr. McKhann reports personal fees from Koh Young Inc.

Figure titles and legends:

Figure 1. IEDs are traveling waves. (**A**) A electron micrograph of an UEA and a picture of an UEA implanted next to an ECoG electrode. (**B**) A raster plot showing an example time course of semi-chronic microelectrode recording during an epilepsy patient's hospital stay. Each gray dot represents the time of one IED (y-axis is arbitrary). (**C**) An example IED recorded across microelectrodes. Each gray line is the same IED recorded on a different microelectrode. The mean IED waveform is overlaid in white. (**D**) Mean spectrogram of the IED shown in (**C**) across microelectrodes. (**E**) A temporally expanded view of the IED shown in (**C**) color coded by when the IED occurs. Black dots indicate the location of the IED negative peaks for each microelectrode. (**F**) A raster plot of IED-associated MUA firing for the same IED as in (**C**) and the same timescale shown in (**F**). (**G**) IED voltage minima timings, color-coded as in (**E**), superimposed across the footprint of the UEA. A white velocity vector derived from the multilinear regression model is also shown on the UEA footprint. (**H**) A polar histogram showing the distribution of all IED traveling waves from which the IED in (**C**) was taken. See Figures S1 and S2 and Algorithm S1 for IED detection and traveling wave classification details.

Figure 2. IED traveling wave distributions are non-uniform and bimodal. (**A**) polar histograms of IED traveling wave directions for all 10 participants. Each participant number is indicated in bold above and to the right of each histogram. (**B**) Classification index for bimodality of IED distributions across subjects. Criterion is indicated with a dashed line. (**C**) Difference in median angles of sub-distributions for bimodal IED distributions, with non-bimodal subjects omitted. See Figure S3 for bimodality classification details.

Figure 3. IEDs reflect ictal self-organization. (**A**) mean voltage recorded across the UEA at the start of a seizure. (**B**) Mean MUA firing rate across microelectrodes. (**C**) A raster plot ordered by time of recruitment and color coded to show the IW (blue) and ictal core ("recruited", pink). (**D**) Slow firing rate dynamics on each microelectrode colored by time of maximum firing rate. (**E**) Times of maximum firing rate on each microelectrode superimposed on the footprint of the UEA, color-coded as in (**D**). (**F**) A polar histogram of IEDs and the direction of the IW. (**G**)

Polar histograms showing probability densities of IEDs and SDs, and the direction of the IW. See Figure S4 for examples of classes of microelectrode array recorded ictal self-organization.

Figure 4. IED and SD distributions in "recruited" UEA recordings. (**A-F**) Each lettered subpanel corresponds to one participant. Each polar histogram corresponds to one seizure. IED distributions are shown in gray and SD distributions are shown in black. Each distribution is plotted relative to the direction of the IW (blue line). (**G**) Direction difference summaries for each seizure ordered and color coded as in (**A-F**). Dots indicate median directions and lines indicate standard deviations. (**H**) Median and standard deviation IED direction summaries relative to median SD directions. See Figure S5 for raw IW, IED, and SD directions.

Figure 5. Correspondence between spatial features of IED and SD sub-distributions. (**A**) Example IED sub-distributions from one participant. (**B**) Example SD sub-distributions from the same participant as in (**A**). Numbers of IEDs in each sub-distribution are displayed in the color of each sub-distribution. (**C**) Mean IED waveforms from each sub-distribution, color coded as in (**A**). (**D**) Mean firing rates from each IED sub-distribution, color coded as in (**A**). (**E**) Scatter and box plots for IED and SD propagation speeds, separated by sub-distribution across subjects, and color coded as in (**A-B**). Boxes indicate median, quartiles, and whiskers indicate 1.5 times the interquartile range. Speeds greater than 350 cm/s are not shown for display purposes. Asterisks indicate significant differences ($p < 0.05$). (**F**) Distribution summaries for IED and SD traveling wave directions, separated by sub-distribution across subjects, and color coded as in (**A-B**). For the two participants with more than one seizure (P4, P6), each seizure is shown separately in (**E**) and (**F**).

Figure 6. Schematic of how IEDs relate to ictal self-organization. A schematic of spatial features of ictal self-organization is shown on the left. Schematics illustrating the correspondence between spatial features (speed, directions, and proportion) of IEDs and SDs is shown on the right.

Tables:

Table 1. Summary statistics for spatiotemporal features of the dataset.

participant	Seizure Class	N detected IEDs	N (%) traveling waves (LFP)	N traveling waves (MUA)	median speed (cm/s)	Bimodal?	N Seizures
1	recruited	1761	1567 (89.0)	640	20.9	yes	1
2	recruited	1532	1217 (79.4)	131	59.2	no	3
3	recruited	17988	10220 (56.8)	10380	25.3	yes	1
4	recruited	2806	1429 (50.9)	284	63.7	yes	1
5	recruited	2148	1538 (71.6)	1131	108.3	yes	2

6	recruited	3502	3143 (89.7)	2006	69	yes	2
7	penumbral	4348	2132 (49.0)	2236	76.8	yes	5
8	penumbral	8369	7351 (87.8)	4977	134.7	no	0
9	penumbral	834	296 (35.5)	50	80.5	yes	3
10	penumbral	2335	1385 (59.3)	322	70.7	yes	4
Totals		45623	30278	22157			22

Data and code availability: Data are available via data use agreement, as required by the Columbia University Medical Center Institutional Review Board. All analysis code is available at https://github.com/elliothsmith/IEDs.

Participants, ethics statement, and data

The data for this study were acquired from Utah-style microelectrode arrays (UEAs) that were implanted in 10 human patients across two surgical sites who were undergoing neurophysiological monitoring for surgical treatment for medically refractory seizures. Clinical details for all participants are shown in Extended Table 1. The Institutional Review Boards at the University of Utah (IRB_00114691) and Columbia University Medical Center (IRB-AAAB6324) approved these studies. All participants provided informed consent prior to surgery for implantation of the clinical electrocorticography (ECoG) electrodes and UEA (10 x 10 electrodes in 4 x 4 mm, penetrating 1 mm). Methodological details of surgical implantation of UEAs into human epilepsy patients area described in detail in House et al. *(House et al., 2006)*. During implantation of ECoG electrodes, UEAs were pneumatically inserted into areas that were most likely to be in the seizure onset zone, and therefore most likely to be resected. Electrophysiological data were pseudodifferentially amplified by 10 and acquired at 30 kilosamples per second using a neural signal processing system (Blackrock Microsystems, Salt Lake City, UT) semi-chronically, that is throughout the duration of the participants' hospital stays. Throughout the manuscript, numerical quantities are presented as mean ± standard deviation (s.d.).

IED detection and signal processing

In order to detect IEDs from continuous data recorded on each UEA channel, we developed a simple algorithm for detecting IEDs across a microelectrode array (Algorithm S1). For each channel on each UEA, we first resampled the data at 400 samples per second and zero-phase filtered the data between 20 and 40 Hz using a 4th order Butterworth filter. We then detected any peaks in the absolute amplitude of this signal that were greater than 8 times the standard deviation of the remainder of the recording segment (2-hour median duration; Fig. S1A). In order to remove redundant detections, those following any other detection by less than 250 ms were discarded. Only detections that occurred within the same 250 ms window across at least 10 electrodes on the

UEA were retained for further analysis (Fig. S1B). Spectrograms of IEDs were generated via the continuous wavelet transform following the methods used in (Schevon et al., 2012b; Smith et al., 2020), and colored with the turbo color map *(Mikhailov, n.d.)*.

Multiunit action potentials (MUA) were detected on each microelectrode by filtering each channel between 0.3 and 3 kilohertz and detecting peaks in the filtered signal less than -4 times its root mean square. The times of these peaks were retained for further analysis. Example retained detections are shown in Fig. S1C-E.

We employed several post-detection processing steps to ensure the quality of this expansive data set, and reject artifacts. First, temporally outlying voltage extrema were removed in order to constrain extrema detection into a temporally focused window (approximately 50 millisecond duration) around the time of IED detection and to exclude broken microelectrodes or those without IED signal. Next, we excluded any discharges with outlying amplitudes, defined as double the interquartile range of the distribution of IED voltage ranges (Fig. S1F-G).

Traveling wave measurement

In order to measure IED traveling wave speed and direction, we fit a plane to the timings of IED voltage minima, and MUA event times, using ordinary multilinear regression, regularized via the absolute deviation of the signal (Fig. S2). This methodology is described in detail and validated for measuring traveling waves during ictal discharges in Liou et al. *(Liou et al., 2017)*. Briefly, the regression model for each IED yielded three coefficients, describing the best-fit plane to the timing of IEDs across the UEA in spacetime. Traveling wave direction was determined by the gradient direction of the plane and speed was defined as the inverse of that gradient norm. Each IED was operationally defined as a traveling wave if its model significantly deviated from a plane with zero slope. Statistical significance for this measure was determined by a permutation test in which the model was reevaluated 1000 times with the microelectrode spatial locations randomly permuted. Differences in IED speed across and within participants were tested using a two-way Kruskal-Wallis Test with a participant factor (10 levels; one for each participant) and a signal factor in which the two levels were the speed measurements derived from LFP and MUA. Only MUA times from 50 ms before and after the median time of the LFP negative peak were included in the regression model *(Liou et al., 2017)*. Post-hoc pairwise comparisons were carried out using Dunn's test *(Dunn, 1964)*. The significance criterion was chosen as 0.05 for all of these tests.

Directional statistics

Polar histograms were plotted using 18 bins. Circular normal distributions were fit using the circular statistics toolbox *(Berens, 2009)*. These distributions defined by two parameters, μ and κ, which describe the central angle and concentration of the distribution, respectively. μ and $1/\kappa$ are analogous to the mean and variance parameters that define a standard normal distribution. Directional statistics were carried out using modified functions from the circular statistics toolbox *(Berens, 2009)*. These modifications were such that statistical significance was evaluated using permutation tests from which p-values were derived by comparing the circular test statistic with a distribution of circular test statistics from 1000 permuted datasets. As an example, testing for differences between IED and SD means would involve comparing the test statistic from the true data to a distribution of 1000 test statistics in which the measurement categories were permuted. The significance criterion was chosen to be 0.05. Hypotheses that within-participant IED propagation directions were non-uniform, were tested with Hermans-Rasson tests of circular non-uniformity, again with 1000 permutations *(Landler et al., 2018)*.

Bimodality and sub-distributions

In order to determine whether two, unimodal distributions better fit the ostensibly bimodal IED and SD distributions we observed, we first fit von Mises Mixture (vMM) Models to overall distributions of IED and SD directions using the Matlab function *fitmvmdist* (https://github.com/chrschy/mvmdist). Overall IED direction distributions were then clustered into two component vMM distributions using the Matlab function *cluster*. We did not observe distributions that appeared to have more than two modes and therefore set an upper limit on the number of hypothesized clusters, h, at two. These vMMs yielded three parameters for each sub-distribution, $h \in \mathbb{N}$, such that $h \leq 2$: the sub-distribution means, μ_h, concentration parameters, κ_h, and probability densities, θ_h.

Rather than assuming these vMM models better fit overall IED and SD distributions, we assessed whether the overall distribution or each vMM sub-distribution better fit the distributions defined by μ_h and κ_h. The permutation-based Kuiper tests used to assess goodness-of-fit were carried out as follows. We first estimated μ_h, κ_h, and θ_h for both the overall and vMM sub-distributions. We then carried out permutation-based Kuiper tests, to compare empirical distributions of 60 randomly sampled IED directions to theoretical circular normal distributions derived from μ_h and κ_h from both the original and vMM sub-distributions. We repeated this procedure 1000 times in order to create a permutation distribution. In this way, we were able to measure the extent to which randomly sampled IED angles deviated from theoretical circular distributions defined by the overall and vMM parameters. This is akin to cross-validating vM parameters and choosing h corresponding to the highest log-likelihood, yet in a model-free way. Comparing Kuiper test statistics to a permutation distribution, rather than zero (the null hypothesis of a uniform distribution), makes the tests more conservative and allows us to determine whether the distribution cannot be determined to be non-normal *(Louter and Koerts, 1970)*. We then defined our circular bimodality index as the minimum difference between the Kuiper test statistic for the overall distribution and each vMM sub-distribution. Positive bimodality indices thus indicated that overall traveling wave distributions were better modeled as two vMM sub-distributions, and negative bimodality indices indicated that overall traveling distributions were better modeled as a single von Mises distribution. The Matlab functions for implementing these classifications are highlighted in the online code repository.

Seizure characterization

In order to study the propagation patterns of IEDs relative to seizures, it was necessary to quantify spatial features of SDs and seizure expansion for each recorded seizure. These measures have also been described in previous publications *(Merricks et al., 2020; Schevon et al., 2012a; Smith et al., 2020, 2016)*. The ictal wavefront is the slowly expanding edge of the seizure representing the spatial signature of failure of feedforward inhibition, and therefore defines recruitment of the tissue surrounding an electrode into the ictal core *(Schevon et al., 2012b)*. This biomarker of seizure recruitment and expansion has thus far only been detected with recordings of multiunit firing rates *(Smith et al., 2016)*, and can also be detected on single microelectrodes by observing widening of action potential waveforms *(Merricks et al., 2020, 2015)*. We followed methods from our previous manuscripts to generate multiunit firing rates, i.e. filtering the broadband data between 300 and 3000 Hz and detecting any peaks larger than the median absolute value of the signal divided by 0.6745 *(Quiroga et al., 2004)*.

For all seizures, we looked for tonic multiunit firing spreading across the array that would suggest the presence of an ictal wavefront, and phase locked multiunit bursting associated with ictal discharges. We detected the ictal wavefront feature of seizures by smoothing the firing rates on each microelectrode with a 250 millisecond Gaussian kernel and fitting a multilinear regression model to the peaks of these slow firing rate estimates across the UEA *(Liou et al., 2017; Smith et al., 2016)*. We detected ictal discharges by detecting peaks in multiunit firing rates, calculated with a 25 millisecond Gaussian kernel, as we have previously *(Liou et al., 2017; Smith et al., 2016)*. We quantified the propagation direction and speed of ictal discharges using the same methods used to determine IED traveling wave speeds and directions, as in Liou et al. *(Liou et al., 2017)*. IED speeds and directions were measured in a manner that was blinded to each microelectrode array's recruitment classification. We defined the presence of ictal phase-locked firing with a Hermans-Rasson test of circular uniformity on MUA action potential times across microelectrodes relative to the phase of the mean LFP recorded across the UEA, similarly to *(Schevon et al., 2012a)*. Using these measures, we operationally defined two patterns of ictal self-organization, based on observed patterns in these fast and slow spatial features of seizures: "recruited" seizures were operationally defined as those with a significant ictal wavefront multilinear regression model and significant phase-locked multiunit firing (Fig. S4A-D). "Penumbral" seizures were operationally defined as those seizures in which we were unable to detect an ictal wavefront on the microelectrode array (Fig. S4E-H). Similar classifications of adjacent and non-adjacent recruitment have been reported by other groups *(Martinet et al., 2015; Schevon et al., 2012b)*. For seizures that were associated with secondary generalization, we only included discharges up to the clinically defined point of secondary generalization in order to constrain our study to the dynamics of focal seizure onset and spread.

Comparing IED and SD sub-distributions

For distributions that were determined to be bimodal, we used cluster-based permutation tests to test for differences between median IED waveforms and firing rates between IEDs from the two component vMM distributions for each participant. Mean firing rates were estimated by binning MUA event times into one-hundred 10-ms bins across microelectrodes. In order to test for different directions of overall distributions and sub-distributions of IEDs and SDs, we used Watson-Williams multi-sample tests for equal means. To test for differences in IED speed between different sub-distributions, we used within-participant Mann-Whitney U tests. In order to test differences in the proportion of IEDs from predominant and auxiliary sub-distributions we used two-sample proportion tests. We employed a significance criterion of 0.05 for all of these tests.

Finally, in order to directly quantify the reduction in uncertainty about the direction of SD travel that can be estimated from observing IED directions, we calculated the Kullback-Leibler Divergence (KLD) between distributions of IED and SD directions *(Kullback and Leibler, 1951)*. We estimated the KLD as the expectation of the logarithmic difference between discrete distributions of IED and SD directions on the half-closed interval between 0 and 2π. We interpret the KLD as measuring the information that can be gained about SD directions from observing IED directions.

Supplemental Materials:

Fig. S1. IED detection and artifact rejection.
Fig. S2. Classifying IED traveling waves.
Fig. S3. Procedures for clustering and evaluating the goodness-of-fit of overall and VonMises mixture distributions.
Fig. S4. Examples of each class of microelectrode seizure recording.
Fig. S5. Raw IED and SD distributions in "recruited" UEA recordings.
Table S1. Clinical details for research participants.
Algorithm S1. IED detection with microelectrode array data.
Movie S1. Video of IEDs and ictal recruitment.

References:

Alarcon G. 1997. Origin and propagation of interictal discharges in the acute electrocorticogram. Implications for pathophysiology and surgical treatment of temporal lobe epilepsy. *Brain* **120**:2259–2282. doi:10.1093/brain/120.12.2259

Baud MO, Kleen JK, Mirro EA, Andrechak JC, King-Stephens D, Chang EF, Rao VR. 2018. Multi-day rhythms modulate seizure risk in epilepsy. *Nat Commun* **9**:88. doi:10.1038/s41467-017-02577-y

Berens P. 2009. CircStat: A MATLAB Toolbox for Circular Statistics. *J Stat Soft* **31**. doi:10.18637/jss.v031.i10

Bi G, Poo M. 1998. Synaptic Modifications in Cultured Hippocampal Neurons: Dependence on Spike Timing, Synaptic Strength, and Postsynaptic Cell Type. *The Journal of Neuroscience* **18**:10464–10472. doi:10.1523/JNEUROSCI.18-24-10464.1998

Conrad EC, Tomlinson SB, Wong JN, Oechsel KF, Shinohara RT, Litt B, Davis KA, Marsh ED. 2020. Spatial distribution of interictal spikes fluctuates over time and localizes seizure onset. *Brain* **143**:554–569. doi:10.1093/brain/awz386

de Curtis M, Jefferys JGR, Avoli M. 2012. Interictal Epileptiform Discharges in Partial Epilepsy In: Noebels J, Avoli M, Rogawski M, Olsen R, Delgado-Escueta A, editors. Jasper's Basic Mechanisms of the Epilepsies. Oxford University Press. pp. 213–227. doi:10.1093/med/9780199746545.003.0017

Dunn OJ. 1964. Multiple Comparisons Using Rank Sums. *Technometrics* **6**:241–252. doi:10.2307/1266041

Eissa TL, Dijkstra K, Brune C, Emerson RG, van Putten MJAM, Goodman RR, McKhann GM, Schevon CA, van Drongelen W, van Gils SA. 2017. Cross-scale effects of neural interactions during human neocortical seizure activity. *Proceedings of the National Academy of Sciences* **114**:10761–10766. doi:10.1073/pnas.1702490114

Fisher R. 1953. Dispersion on a Sphere. *Proceedings of the Royal Society A: Mathematical, Physical and Engineering Sciences* **217**:295–305. doi:10.1098/rspa.1953.0064

Gelinas JN, Khodagholy D, Thesen T, Devinsky O, Buzsáki G. 2016. Interictal epileptiform discharges induce hippocampal–cortical coupling in temporal lobe epilepsy. *Nature Medicine* **22**:641–648. doi:10.1038/nm.4084

House PA, MacDonald JD, Tresco PA, Normann RA. 2006. Acute microelectrode array implantation into human neocortex: preliminary technique and histological considerations. *Neurosurgical focus* **20**:1–4.

Keller CJ, Truccolo W, Gale JT, Eskandar E, Thesen T, Carlson C, Devinsky O, Kuzniecky R, Doyle WK, Madsen JR, Schomer DL, Mehta AD, Brown EN, Hochberg LR, Ulbert I, Halgren E, Cash SS. 2010. Heterogeneous neuronal firing patterns during interictal epileptiform discharges in the human cortex. *Brain* **133**:1668–1681. doi:10.1093/brain/awq112

Khodagholy D, Gelinas JN, Thesen T, Doyle W, Devinsky O, Malliaras GG, Buzsáki G. 2014. NeuroGrid: recording action potentials from the surface of the brain. *Nature Neuroscience* **18**:310.

Kim DW, Kim HK, Lee SK, Chu K, Chung CK. 2010. Extent of neocortical resection and surgical outcome of epilepsy: Intracranial EEG analysis. *Epilepsia* **51**:1010–1017. doi:https://doi.org/10.1111/j.1528-1167.2010.02567.x

Kullback S, Leibler RA. 1951. On Information and Sufficiency. *The Annals of Mathematical Statistics* **22**:79–86. doi:10.1214/aoms/1177729694

Landler L, Ruxton GD, Malkemper EP. 2018. Circular data in biology: advice for effectively implementing statistical procedures. *Behav Ecol Sociobiol* **72**. doi:10.1007/s00265-018-2538-y

Liou J, Smith EH, Bateman LM, Bruce SL, McKhann GM, Goodman RR, Emerson RG, Schevon CA, Abbott L. 2020. A model for focal seizure onset, propagation, evolution, and progression. *eLife* **9**:e50927. doi:10.7554/eLife.50927

Liou J, Smith EH, Bateman LM, McKhann GM, Goodman RR, Greger B, Davis TS, Kellis SS, House PA, Schevon CA. 2017. Multivariate regression methods for estimating velocity of ictal discharges from human microelectrode recordings. *Journal of Neural Engineering* **14**:044001. doi:10.1088/1741-2552/aa68a6

Liou J-Y, Baird-Daniel E, Zhao M, Daniel A, Schevon CA, Ma H, Schwartz TH. 2019. Burst suppression uncovers rapid widespread alterations in network excitability caused by an acute seizure focus. *Brain* **142**:3045–3058. doi:10.1093/brain/awz246

Louter AS, Koerts J. 1970. On the Kuiper test for normality with mean and variance unknown. *Statistica Neerlandica* **24**:83–87. doi:https://doi.org/10.1111/j.1467-9574.1970.tb00110.x

Marsh ED, Peltzer B, Brown MW, Wusthoff C, Storm PB, Litt B, Porter BE. 2010. Interictal EEG spikes identify the region of seizure onset in some, but not all pediatric epilepsy patients. *Epilepsia* **51**:592–601. doi:10.1111/j.1528-1167.2009.02306.x

Martinet L-E, Ahmed OJ, Lepage KQ, Cash SS, Kramer MA. 2015. Slow Spatial Recruitment of Neocortex during Secondarily Generalized Seizures and Its Relation to Surgical Outcome. *Journal of Neuroscience* **35**:9477–9490. doi:10.1523/JNEUROSCI.0049-15.2015

Martinet L-E, Fiddyment G, Madsen JR, Eskandar EN, Truccolo W, Eden UT, Cash SS, Kramer MA. 2017. Human seizures couple across spatial scales through travelling wave dynamics. *Nature Communications* **8**:14896. doi:10.1038/ncomms14896

Merricks EM, Smith EH, Emerson RG, Bateman LM, McKhann GM, Goodman RR, Sheth SA, Greger B, House PA, Trevelyan AJ, Schevon CA. 2020. Neuronal firing and waveform alterations through ictal recruitment in humans. *J Neurosci*. doi:10.1523/JNEUROSCI.0417-20.2020

Merricks EM, Smith EH, McKhann GM, Goodman RR, Bateman LM, Emerson RG, Schevon CA, Trevelyan AJ. 2015. Single unit action potentials in humans and the effect of seizure activity. *Brain* **138**:2891–2906. doi:10.1093/brain/awv208

Mikhailov A. n.d. Turbo, An Improved Rainbow Colormap for Visualization. *Google AI Blog*.

Muller L, Piantoni G, Koller D, Cash SS, Halgren E, Sejnowski TJ. 2016. Rotating waves during human sleep spindles organize global patterns of activity that repeat precisely through the night. *eLife* **5**:e17267. doi:10.7554/eLife.17267

Nguyen Q-A, Moolchand P, Soltesz I. 2020. Connecting Pathological Cellular Mechanisms to Large-Scale Seizure Structures. *Trends in Neurosciences* **43**:547–549. doi:10.1016/j.tins.2020.04.006

Paolicchi JM, Jayakar P, Dean P, Yaylali I, Morrison G, Prats A, Resnik T, Alvarez L, Duchowny M. 2000. Predictors of outcome in pediatric epilepsy surgery. *Neurology* **54**:642–642. doi:10.1212/WNL.54.3.642

Quiroga RQ, Nadasdy Z, Ben-Shaul Y. 2004. Unsupervised Spike Detection and Sorting with Wavelets and Superparamagnetic Clustering. *Neural Computation* **16**:1661–1687. doi:10.1162/089976604774201631

Schevon CA, Weiss SA, McKhann G, Goodman RR, Yuste R, Emerson RG, Trevelyan AJ. 2012a. Evidence of an inhibitory restraint of seizure activity in humans. *Nat Commun* **3**:1060. doi:10.1038/ncomms2056

Schevon CA, Weiss SA, McKhann Jr G, Goodman RR, Yuste R, Emerson RG, Trevelyan AJ. 2012b. Evidence of an inhibitory restraint of seizure activity in humans. *Nature Communications* **3**:1060.

Smart O, Maus D, Marsh E, Dlugos D, Litt B, Meador K. 2012. Mapping and mining interictal pathological gamma (30–100Hz) oscillations with clinical intracranial EEG in patients with epilepsy. *Expert Systems with Applications* **39**:7355–7370. doi:10.1016/j.eswa.2012.01.071

Smith EH, Liou J, Davis TS, Merricks EM, Kellis SS, Weiss SA, Greger B, House PA, McKhann II GM, Goodman RR, Emerson RG, Bateman LM, Trevelyan AJ, Schevon CA. 2016. The ictal wavefront is the spatiotemporal source of discharges during spontaneous human seizures. *Nature Communications* **7**:11098.

Smith EH, Merricks EM, Liou J-Y, Casadei C, Melloni L, Thesen T, Friedman DJ, Doyle WK, Emerson RG, Goodman RR, McKhann GM, Sheth SA, Rolston JD, Schevon CA. 2020. Dual mechanisms of ictal high frequency oscillations in human rhythmic onset seizures. *Scientific Reports* **10**:19166. doi:10.1038/s41598-020-76138-7

Staley KJ, White A, Dudek FE. 2011. Interictal spikes: harbingers or causes of epilepsy? *Neurosci Lett* **497**:247–250. doi:10.1016/j.neulet.2011.03.070

Tatum WO, Selioutski O, Ochoa JG, Clary HM, Cheek J, Drislane FW, Tsuchida TN. 2016. American Clinical Neurophysiology Society Guideline 7: Guidelines for EEG Reporting. *The Neurodiagnostic Journal* **56**:285–293. doi:10.1080/21646821.2016.1245576

Tonini C, Beghi E, Berg AT, Bogliun G, Giordano L, Newton RW, Tetto A, Vitelli E, Vitezic D, Wiebe S. 2004. Predictors of epilepsy surgery outcome: a meta-analysis. *Epilepsy Research* **62**:75–87. doi:10.1016/j.eplepsyres.2004.08.006

Trevelyan AJ, Sussillo D, Watson BO, Yuste R. 2006. Modular Propagation of Epileptiform Activity: Evidence for an Inhibitory Veto in Neocortex. *Journal of Neuroscience* **26**:12447–12455. doi:10.1523/JNEUROSCI.2787-06.2006

Trevelyan AJ, Sussillo D, Yuste R. 2007. Feedforward Inhibition Contributes to the Control of Epileptiform Propagation Speed. *Journal of Neuroscience* **27**:3383–3387. doi:10.1523/JNEUROSCI.0145-07.2007

Vakharia VN, Duncan JS, Witt J-A, Elger CE, Staba R, Engel J. 2018. Getting the best outcomes from epilepsy surgery. *Annals of Neurology* **83**:676–690. doi:https://doi.org/10.1002/ana.25205

Viventi J, Kim D-H, Vigeland L, Frechette ES, Blanco JA, Kim Y-S, Avrin AE, Tiruvadi VR, Hwang S-W, Vanleer AC, Wulsin DF, Davis K, Gelber CE, Palmer L, Van der Spiegel J, Wu J, Xiao J, Huang Y, Contreras D, Rogers JA, Litt B. 2011. Flexible, foldable, actively multiplexed, high-density electrode array for mapping brain activity in vivo. *Nature Neuroscience* **14**:1599–1605. doi:10.1038/nn.2973

Weiss SA, Banks GP, McKhann GM, Goodman RR, Emerson RG, Trevelyan AJ, Schevon CA. 2013. Ictal high frequency oscillations distinguish two types of seizure territories in humans. *Brain* **136**:3796–3808. doi:10.1093/brain/awt276

Wenzel M, Hamm JP, Peterka DS, Yuste R. 2017. Reliable and Elastic Propagation of Cortical Seizures In Vivo. *Cell Reports* **19**:2681–2693. doi:10.1016/j.celrep.2017.05.090

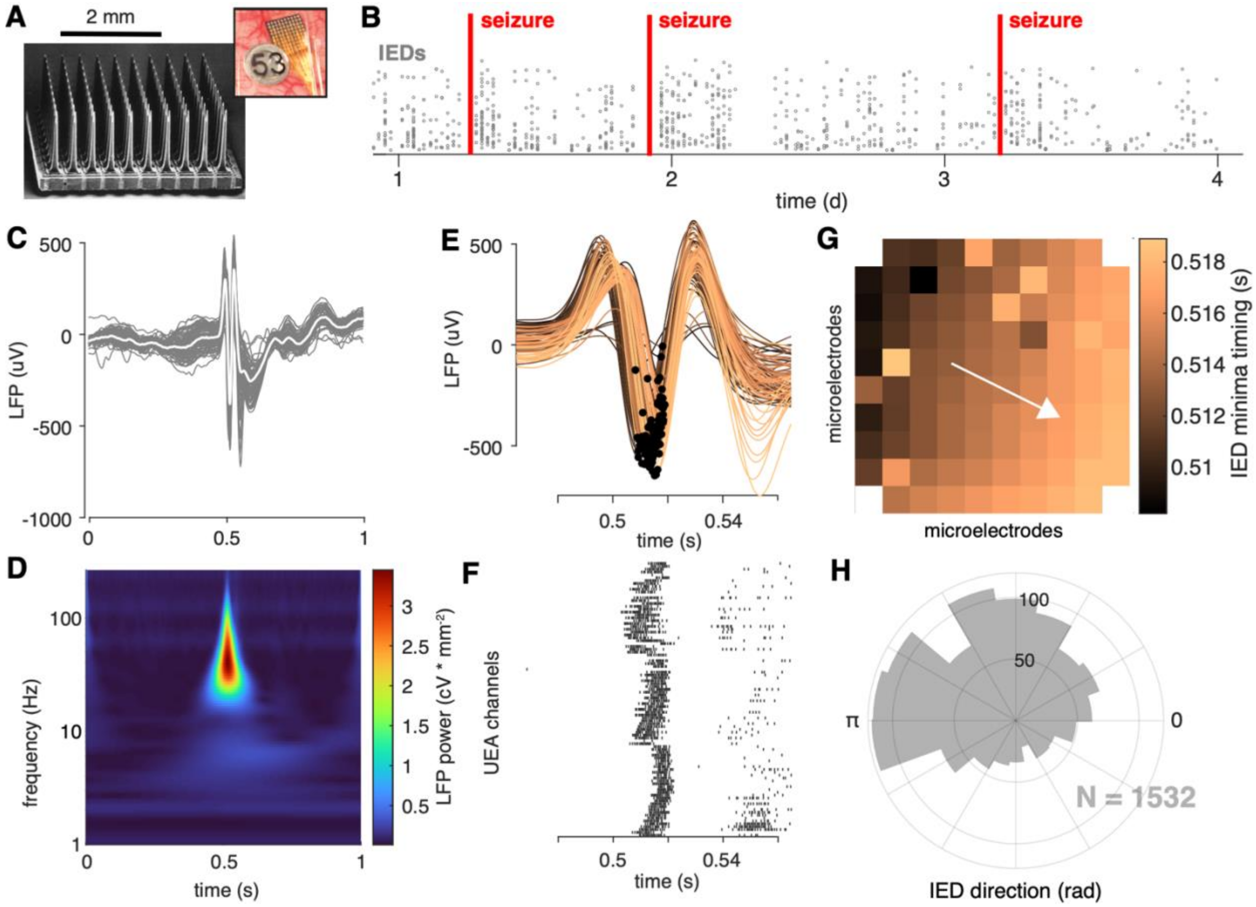
A
2 mm
53
B
seizure
seizure
seizure
IEDs
1
2
3
4
time (d)
C
500
0
-500
-1000
LFP (uV)
0
0.5
1
E
500
0
-500
LFP (uV)
0.5
0.54
time (s)
G
microelectrodes
microelectrodes
0.518
0.516
0.514
0.512
0.51
IED minima timing (s)
D
100
10
1
frequency (Hz)
0
0.5
1
time (s)
3
2.5
2
1.5
1
0.5
LFP power (cV * mm²)
F
UEA channels
0.5
0.54
time (s)
H
100
50
π
0
N = 1532
IED direction (rad)

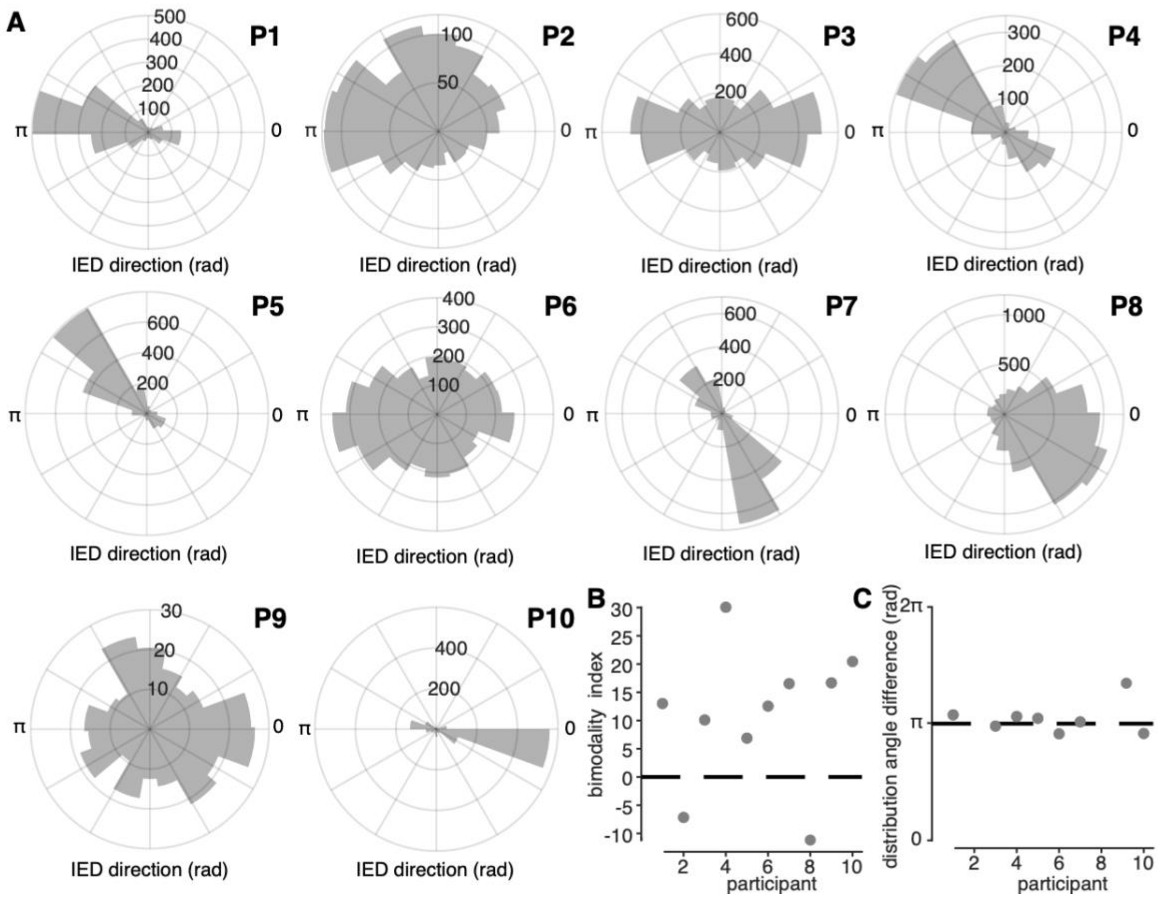
A
P1
P2
P3
P4
P5
P6
P7
P8
P9
P10
IED direction (rad)
π
0
B
bimodality index
participant
C
distribution angle difference (rad)
2π
participant

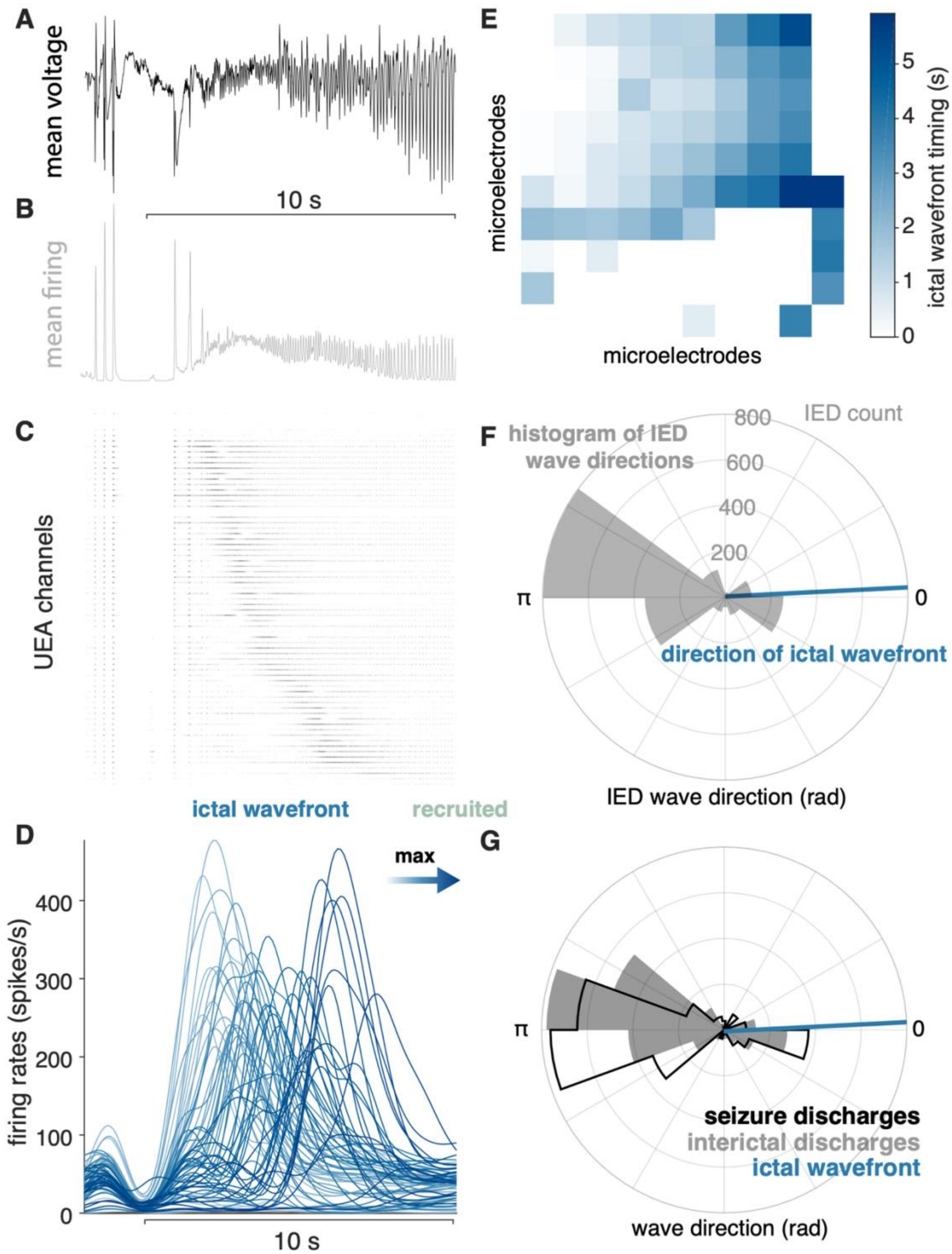
A
mean voltage
B
10 s
mean firing
C
UEA channels
D
ictal wavefront
recruited
max
firing rates (spikes/s)
400
300
200
100
0
10 s
E
microelectrodes
microelectrodes
ictal wavefront timing (s)
5
4
3
2
1
0
F
histogram of IED wave directions
IED count
800
600
400
200
π
0
direction of ictal wavefront
IED wave direction (rad)
G
π
0
seizure discharges
interictal discharges
ictal wavefront
wave direction (rad)

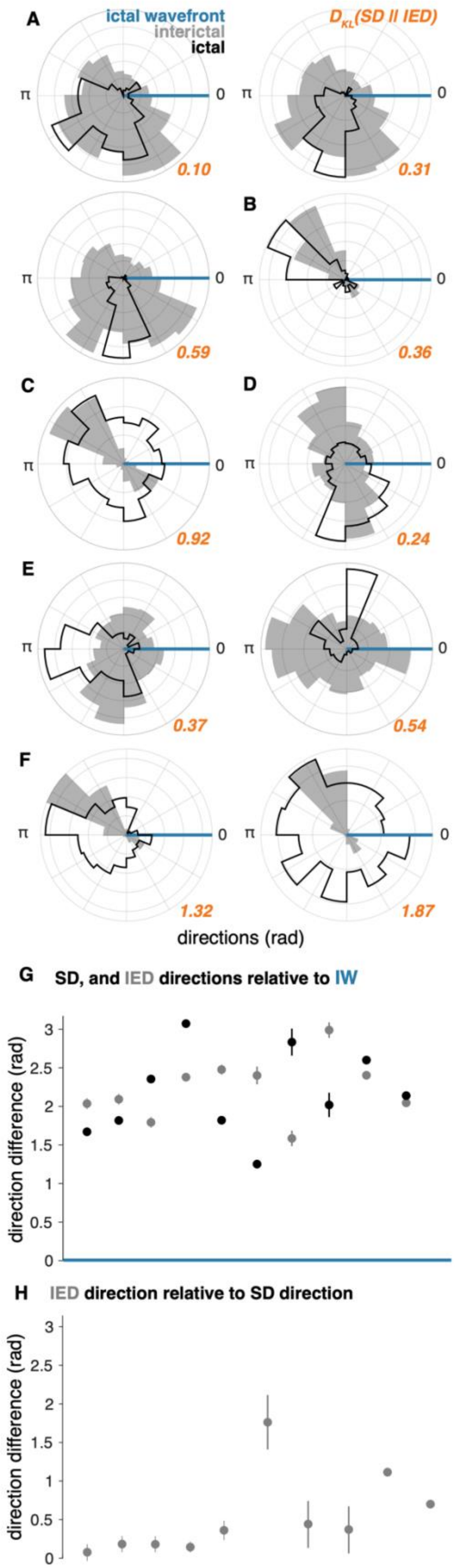
A
ictal wavefront
interictal
ictal
D_KL(SD II IED)
0.10
0.31
B
0.59
0.36
C
D
0.92
0.24
E
0.37
0.54
F
1.32
1.87
directions (rad)
G SD, and IED directions relative to IW
direction difference (rad)
H IED direction relative to SD direction
direction difference (rad)

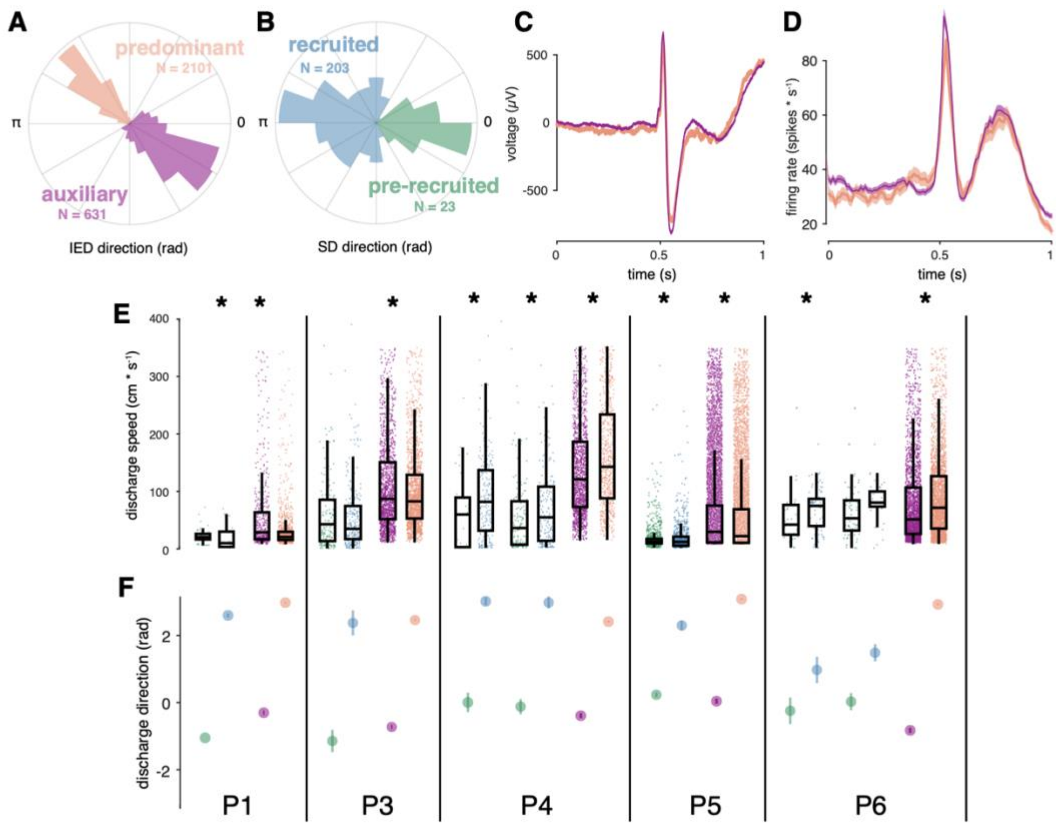
A
predominant
N = 2101
auxiliary
N = 631
π
0
IED direction (rad)
B
recruited
N = 203
pre-recruited
N = 23
π
0
SD direction (rad)
C
voltage (μV)
500
0
-500
time (s)
0
0.5
1
D
firing rate (spikes * s⁻¹)
80
60
40
20
time (s)
0
0.5
1
E
discharge speed (cm * s⁻¹)
400
300
200
100
0
*
F
discharge direction (rad)
2
0
-2
P1
P3
P4
P5
P6

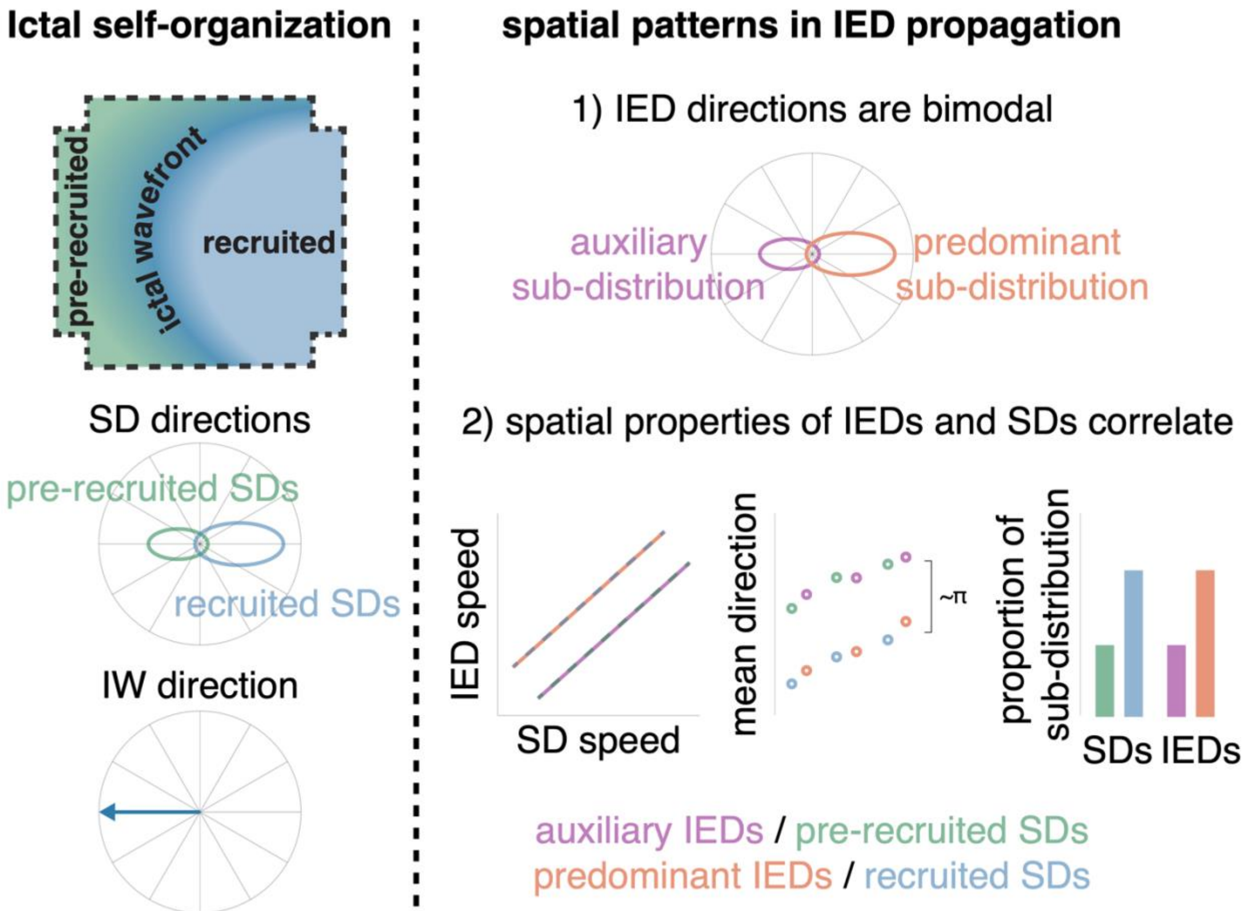
Ictal self-organization
pre-recruited
ictal wavefront
recruited
SD directions
pre-recruited SDs
recruited SDs
IW direction
spatial patterns in IED propagation
1) IED directions are bimodal
auxiliary sub-distribution
predominant sub-distribution
2) spatial properties of IEDs and SDs correlate
IED speed
SD speed
mean direction
~π
proportion of sub-distribution
SDs
IEDs
auxiliary IEDs / pre-recruited SDs
predominant IEDs / recruited SDs

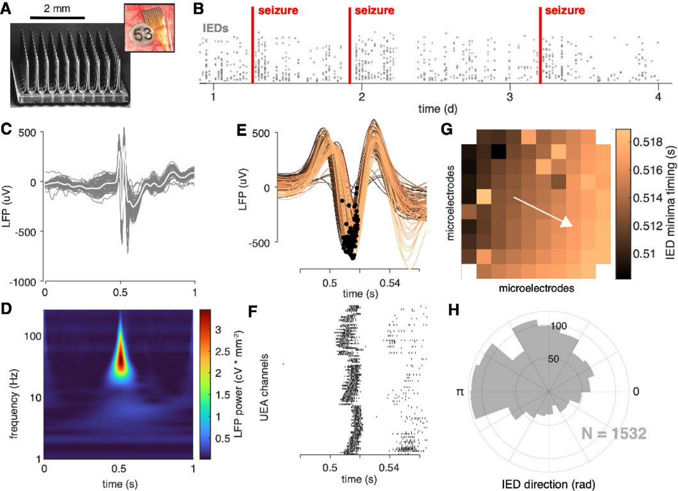

A
2 mm
53
B
seizure
seizure
seizure
IEDs
1
2
3
4
time (d)
C
LFP (uV)
500
0
-500
-1000
0
0.5
1
D
frequency (Hz)
100
10
1
0
0.5
1
time (s)
LFP power (cV * mm²)
3
2.5
2
1.5
1
0.5
E
LFP (uV)
500
0
-500
0.5
0.54
time (s)
F
UEA channels
0.5
0.54
time (s)
G
microelectrodes
microelectrodes
IED minima timing (s)
0.518
0.516
0.514
0.512
0.51
H
100
50
π
0
N = 1532
IED direction (rad)

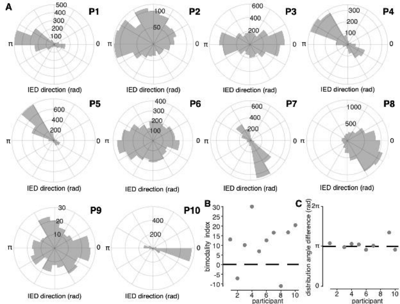
A
P1
500
400
300
200
100
π
0
IED direction (rad)
P2
100
50
π
0
IED direction (rad)
P3
600
400
200
π
0
IED direction (rad)
P4
300
200
100
π
0
IED direction (rad)
P5
600
400
200
π
0
IED direction (rad)
P6
400
300
200
100
π
0
IED direction (rad)
P7
600
400
200
π
0
IED direction (rad)
P8
1000
500
π
0
IED direction (rad)
P9
30
20
10
π
0
IED direction (rad)
P10
400
200
π
0
IED direction (rad)
B
bimodality index
30
25
20
15
10
5
0
-5
-10
2
4
6
8
10
participant
C
distribution angle difference (rad)
2π
π
0
2
4
6
8
10
participant

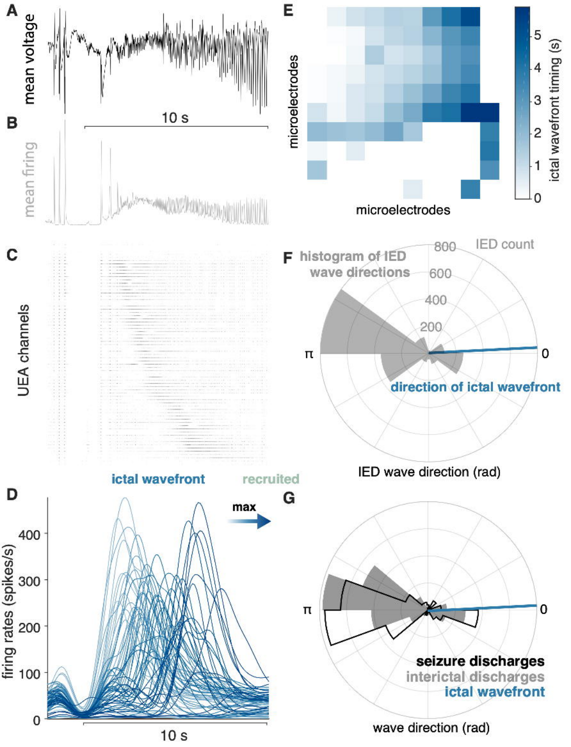
A
mean voltage
10 s
B
mean firing
C
UEA channels
D
ictal wavefront
recruited
max
firing rates (spikes/s)
400
300
200
100
0
10 s
E
microelectrodes
microelectrodes
ictal wavefront timing (s)
5
4
3
2
1
0
F
histogram of IED wave directions
IED count
800
600
400
200
π
0
direction of ictal wavefront
IED wave direction (rad)
G
π
0
seizure discharges
interictal discharges
ictal wavefront
wave direction (rad)

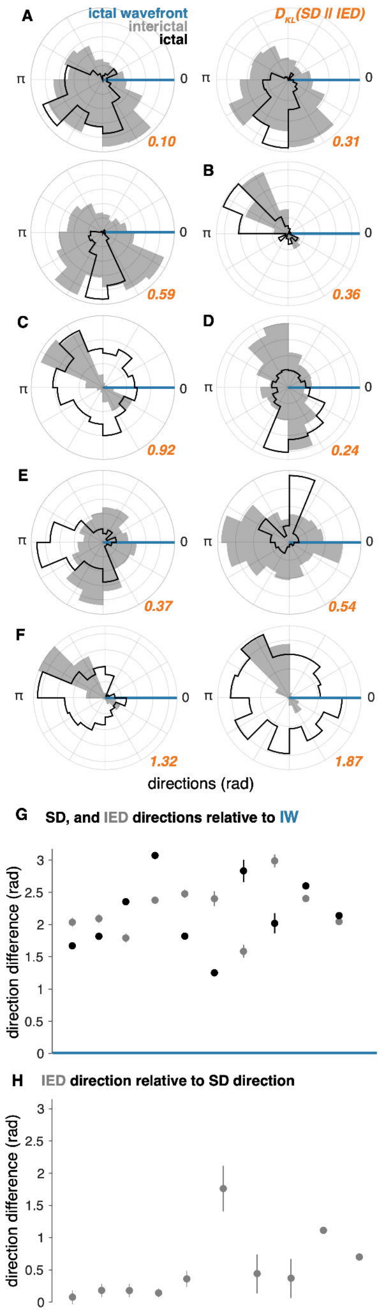
A
ictal wavefront
interictal
ictal
$D_{KL}(SD \parallel IED)$
π
0
0.10
0.31
B
0.59
0.36
C
D
0.92
0.24
E
0.37
0.54
F
1.32
1.87
directions (rad)
G
SD, and IED directions relative to IW
direction difference (rad)
0
0.5
1
1.5
2
2.5
3
H
IED direction relative to SD direction
direction difference (rad)

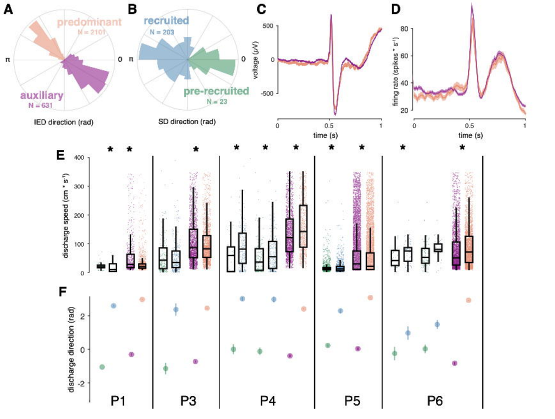
A
predominant
N = 2101
π
0
auxiliary
N = 631
IED direction (rad)
B
recruited
N = 203
pre-recruited
N = 23
SD direction (rad)
C
voltage (μV)
time (s)
D
firing rate (spikes * s⁻¹)
time (s)
E
discharge speed (cm * s⁻¹)
F
discharge direction (rad)
P1
P3
P4
P5
P6

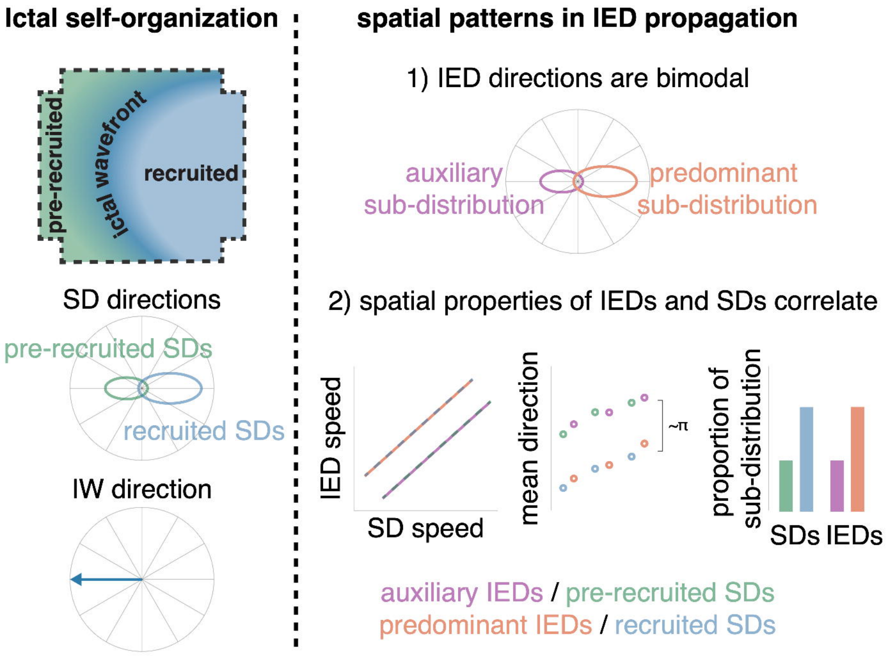
Ictal self-organization
pre-recruited
ictal wavefront
recruited
SD directions
pre-recruited SDs
recruited SDs
IW direction
spatial patterns in IED propagation
1) IED directions are bimodal
auxiliary sub-distribution
predominant sub-distribution
2) spatial properties of IEDs and SDs correlate
IED speed
SD speed
mean direction
~π
proportion of sub-distribution
SDs IEDs
auxiliary IEDs / pre-recruited SDs
predominant IEDs / recruited SDs